View metadata, citation and similar papers at core.ac.uk

brought to you by CORE

provided by Tokushima University Institutional Repository

© 2015. This manuscript version is made available under the CC-BY-NC-ND 4.0 license http://creativecommons.org/licenses/by-nc-nd/4.0/
The published version is available via https://doi.org/10.1016/j.chaos.2015.06.014

A computation method for non-autonomous systems with discontinuous characteristics

Yuu Miino

Advanced Tech. and Science, System Innovation Engineering, Tokushima University,
2–1 Minami-Josanjima, Tokushima
770–8506, Japan
c501437041@tokushima-u.ac.jp

Daisuke Ito

Dept. of Electronic Systems Engineering, School of Engineering, The University of Shiga Prefecture,
2500 Hassaka-cho, Hikone, Shiga
522-8533, Japan
ito.d@e.usp.ac.jp

Tetsushi Ueta

Center for Admin. Info. Tech. Tokushima University,
2–1 Minami-Josanjima, Tokushima
770–8506, Japan
ueta@tokushima-u.ac.jp

Abstract

We propose a computation method to obtain bifurcation sets of periodic solutions in non-autonomous systems with discontinuous properties. If the system has discontinuity for the states and/or the vector field, conventional methods cannot be applied. We have developed a method for autonomous systems with discontinuity by taking the Poincaré mapping on the switching point in the preceded study, however, this idea does not work well for some non-autonomous systems with discontinuity. We overcome this difficulty by extending the system to an autonomous system. As a result, bifurcation sets of periodic solutions are solved accurately with a shooting method. We show two numerical examples and demonstrate the corresponding laboratory experiment.

Keywords: bifurcation phenomena, numerical analysis, nonlinear non-autonomous system, discontinuity

1. Introduction

To analyze stability or bifurcations for a periodic solution of an ordinary differential equation (ODE) with smooth nonlinear characteristics, a bunch of computational packages or algorithms are available[1][2][3]. Basically these methods convert the periodic motion into a fixed point problem by taking Poincaré map and solve it by applying an appropriate shooting method.

On the other hand, if the system contains non-smooth properties, some special treatments should be considered since continuousness of the map for the given ODE is lost [4][5][6], Fortunately some non-smooth systems can be analyzed by putting an approximated smooth function into the ODE. Otherwise, defining a composite Poincaré map with multiple sections attached to break points is required[7]. How to construct the differentiable Poincaré map whose characteristic equation results correct multipliers is a key point of these methods. Previous study[8] showed bifurcation analysis of behaviors on the stepping motor which has an autonomous dynamical system and has discontinuity on its vector field. Another one[9] showed global bifurcation analysis of such systems. However, as far as we know, there are no bifurcation analysis for non-autonomous systems with discontinuity, thus we focus on these systems. In fact, if we apply Kousaka's method which is for autonomous systems to these non-autonomous systems, the shooting method converges slowly and leaves some errors. Thereby tracing bifurcation sets sometimes fails because of accumulation of these errors. We intuitively guess that some special treatment for adding a forcing term in evaluation of the Jacobian matrix.

At first, we tried applying previously mentioned method[7] simply to the forced Izhikevich neuron model[10], which is a non-autonomous system with discontinuity, but then we obtained the differentiable Poincaré map with some errors. The error could not be ignored to analyze bifurcation structure of the system.

In this paper, we investigate a cause of the errors and propose a universal algorithm for solving bifurcation problems of nonlinear non-autonomous hybrid

systems. The remaining contents are organized as follows; Section 2 describes the problem formulation, Section 3 investigates what is a cause of the errors with numerical experiments and propose our idea to solve it. Section 4 devotes to show validation of our method with two examples, i.e., we discuss agreement among computed bifurcation diagrams, numerical solutions, and laboratory experiments of each system. Section 5 concludes our study.

2. Numerical analysis of nonlinear non-autonomous system with discontinuous characteristic

As proposed on the previous study[11], when we consider systems with discontinuous characteristics, we often define the Poincaré section with the condition of discontinuity. However on smooth non-autonomous systems, we often define the Poincaré section with the time because periodic solutions have a periodicity synchronized with the frequency of the external force. Thus on this paper we define the Poincaré section of the systems with the time and try to analyze it by previously mentioned method.

Similarly to the previous study[12], let us consider an n-dimensional non-autonomous system with m-tuple differential equations described by

$$\begin{aligned} \boldsymbol{x} &= (x_1 \dots x_n)^\top \in \boldsymbol{R}^n, & (1)\\ \frac{d\boldsymbol{x}}{dt} &= \boldsymbol{f}_i(t, \boldsymbol{x}), \quad i = 0, \cdots, m-1, & (2) \end{aligned}$$

where $t \in \boldsymbol{S}^1$ is the adjusted time with $\boldsymbol{S}^1 = \{t \in \boldsymbol{R} \mod \tau\}$, $\tau \in \boldsymbol{R}$, which is often $2\pi/\omega$, is a parameter for an initial section Π_0, $\boldsymbol{x} \in \boldsymbol{R}^n$ is the state and $\boldsymbol{f}_i : \boldsymbol{R}^n \to \boldsymbol{R}^n$ is a C^∞ class function.

Assume that there is a periodic solution for Eq. (2). When we suppose that Π_i is a traversal section to the solution orbit and put $\boldsymbol{x}_0 = \boldsymbol{x}(0) \in \Pi_0$, then the solution of Eq. (2) is given by

$$\boldsymbol{x}(t) = \boldsymbol{\varphi}(t, \boldsymbol{x}_0). \quad (3)$$

Moreover, each solution following $\boldsymbol{f}_i$ is given by $\boldsymbol{\varphi}_i(t, \boldsymbol{x}_i, t_i)$, where t_i is the starting time of the solution. Now we provide Π_i with threshold values as follows:

$$\Pi_i = \left\{ t \in \boldsymbol{S}^1, \boldsymbol{x} \in \boldsymbol{R}^n \mid q_i(t, \boldsymbol{x}, \lambda_i) = 0 \right\}, \tag{4}$$

where q_i is a differentiable scalar function and $\lambda_i \in \boldsymbol{R}$ is a unique parameter that defines the position of Π_i. In addition, on the non-autonomous system,

$$\Pi_0 = \left\{ t \in \boldsymbol{S}^1, \boldsymbol{x} \in \boldsymbol{R}^n \mid q_0(t, \boldsymbol{x}, \tau) = t = 0 \right\}, \tag{5}$$

When an orbit governed by $\boldsymbol{f}_i$ reaches the section Π_{i+1}, the governing function is changed to $\boldsymbol{f}_{i+1}$. If the orbit passing through several sections reaches Π_0 again, then m sub maps are defined as follows:

$$\begin{aligned}
T_0 \quad &: \quad \Pi_0 \to \Pi_1 \\
&\quad\;\; \boldsymbol{x}_0 \mapsto \boldsymbol{x}_1 = \boldsymbol{\varphi}_0 \left(t_1, \boldsymbol{x}_0, t_0 = 0 \right) \\
T_1 \quad &: \quad \Pi_1 \to \Pi_2 \\
&\quad\;\; \boldsymbol{x}_1 \mapsto \boldsymbol{x}_2 = \boldsymbol{\varphi}_1 \left(t_2, \boldsymbol{x}_1, t_1 \right) \\
&\quad\;\; \vdots \\
T_{m-1} \quad &: \quad \Pi_{m-1} \to \Pi_0 \\
&\quad\;\; \boldsymbol{x}_{m-1} \mapsto \boldsymbol{x}_m = \boldsymbol{\varphi}_{m-1} \left(t_m, \boldsymbol{x}_{m-1}, t_{m-1} \right).
\end{aligned} \tag{6}$$

From Eq. (6), the Poincaré map T is given by the following composite map:

$$T(\boldsymbol{x}(k), \tau, \lambda_1, \ldots, \lambda_{m-1}) = T_{m-1} \circ \cdots \circ T_1 \circ T_0. \tag{7}$$

Hence

$$\boldsymbol{x}(k+1) = T(\boldsymbol{x}(k), \tau, \lambda_1, \ldots, \lambda_{m-1}). \tag{8}$$

When the orbit starting from $\boldsymbol{x}_0 \in \Pi_0$ returns $\boldsymbol{x}_0$ itself, this orbit forms a periodic orbit and the corresponding fixed point of T is written as follows:

$$\boldsymbol{x}_0 = T(\boldsymbol{x}_0, \tau, \lambda_1, \ldots, \lambda_{m-1}). \tag{9}$$

The characteristic equation is given by

$$\chi(\mu) = \det\left(\frac{\partial T(\boldsymbol{x}_0)}{\partial \boldsymbol{x}_0} - \mu I\right) = 0, \tag{10}$$

where μ is a multiplier of $\partial T(\boldsymbol{x}_0)/\partial \boldsymbol{x}_0$. When the multiplier satisfies $|\mu| = 1$, solution attractors of the system occurs bifurcation phenomena. In other words, μ can be given as $|\mu| = 1$ to obtain a bifurcation parameter set.

3. Problem and solution idea

3.1. Problem on numerical analysis

Here we found a problem on numerical analysis previously mentioned. In common for the systems with discontinuous characteristics, we could use composition of maps for $\partial T/\partial \boldsymbol{x}_0$ as:

$$\frac{\partial T}{\partial \boldsymbol{x}_0} = \prod_{i=0}^{m-1} \frac{\partial T_{m-1-i}}{\partial \boldsymbol{x}_{m-1-i}}\bigg|_{t_{m-1-i}}^{t_{m-i}}. \tag{11}$$

However on numerical experiment, right hand of Eq. (11) is not equal to its left hand of it. Now we confirm this with an example of 1-periodic orbit observed in forced Izhikevich neuron model introduced in Sec.4.1, see Fig. 1.

By using numerical differentiation, we can obtain $\partial T_i/\partial \boldsymbol{x}_i$ roughly:

$$\frac{\partial T_0}{\partial \boldsymbol{x}_0} = \begin{pmatrix} 0.00000 & 0.00000 \\ -0.05423 & 0.70627 \end{pmatrix}, \tag{12}$$

$$\frac{\partial T_1}{\partial \boldsymbol{x}_1} = \begin{pmatrix} 0.00000 & 0.00000 \\ 1.00000 & 1.00000 \end{pmatrix}, \tag{13}$$

$$\frac{\partial T_2}{\partial \boldsymbol{x}_2} = \begin{pmatrix} -0.99281 & 0.36780 \\ 0.24401 & -0.09478 \end{pmatrix}, \tag{14}$$

and for this example, we can regard $m = 3$ and then Eq. (11) is expressed by

$$\frac{\partial T}{\partial \boldsymbol{x}_0} = \frac{\partial T_2}{\partial \boldsymbol{x}_2} \cdot \frac{\partial T_1}{\partial \boldsymbol{x}_1} \cdot \frac{\partial T_0}{\partial \boldsymbol{x}_0}. \tag{15}$$

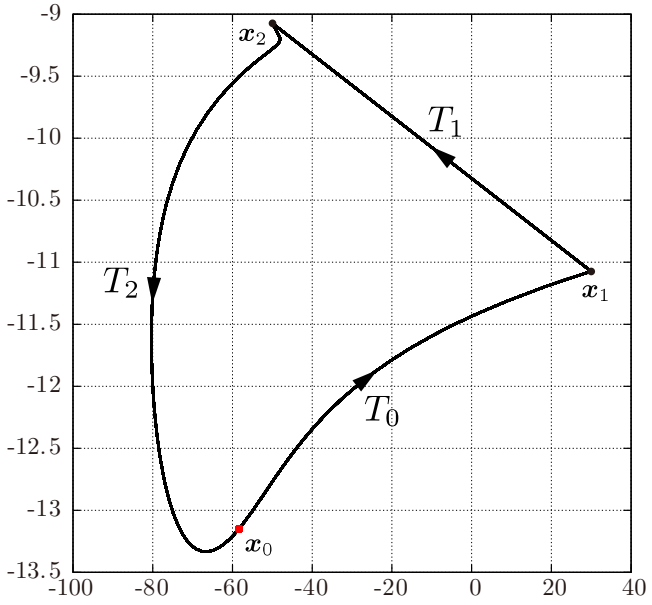

Figure 1: A phase portrait of 1-periodic orbit observed in forced Izhikevich neuron model.

Hence the right hand of Eq. (15) is calculated as

$$\frac{\partial T_2}{\partial \boldsymbol{x}_2} \cdot \frac{\partial T_1}{\partial \boldsymbol{x}_1} \cdot \frac{\partial T_0}{\partial \boldsymbol{x}_0} = \begin{pmatrix} -0.01994 & 0.25977 \\ 0.00514 & -0.06694 \end{pmatrix}. \tag{16}$$

However the characteristic equation according to Eq. (16) does not have correct multipliers.

To investigate a reason of this problem, we focus on the relation between the map T and the time t, and between the time t and the initial value $\boldsymbol{x}_0$ on non-autonomous nonlinear discontinuous systems. On autonomous systems with discontinuous characteristics, $\partial T/\partial \boldsymbol{x}_0 = (\partial T_1/\partial \boldsymbol{x}_1) \cdot (\partial T_0/\partial \boldsymbol{x}_0)$ is satisfied because the map T_1 is assumed to depend only on the initial value $\boldsymbol{x}_1$ and thus the map has been defined as $T_1(\boldsymbol{x}_1) = \boldsymbol{x}_2$. In fact in autonomous systems, a solution orbit is not invariant for the starting time because vector fields of the system does not depend on the starting time. This is because the ODE of such system dose not include the time term explicitly. However on non-autonomous

systems, the map T_1 also depends on the starting time t_1 as shown in (6) and then the map is defined as $T_1(t_1, \boldsymbol{x}_1) = \boldsymbol{x}_2$. The reason is that solution orbits of the system are varied with the starting time because ODEs of non-autonomous systems include the time term explicitly and vector fields spanned by the system depend on the time.

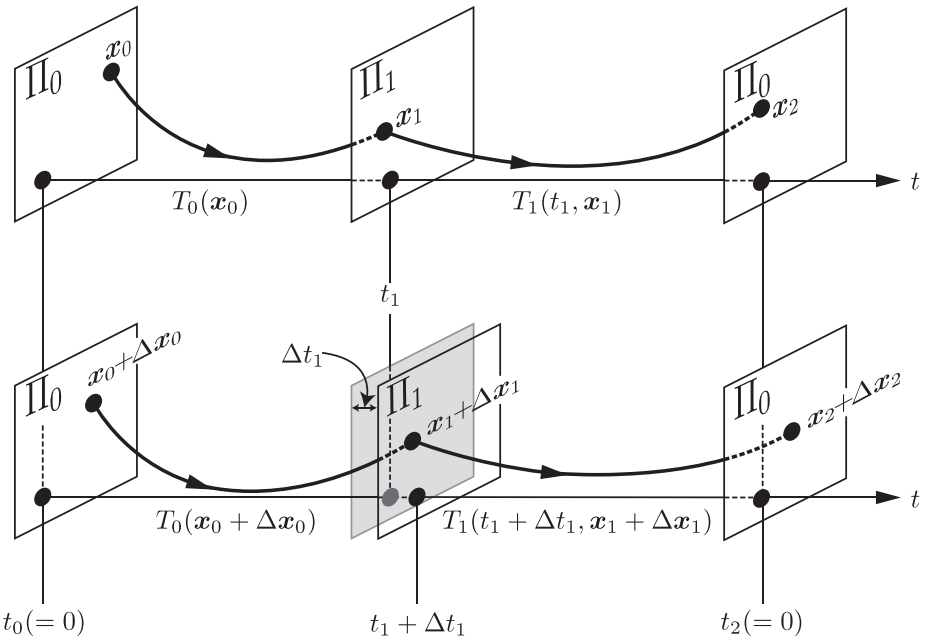

Figure 2: A conceptual figure describing how $\Delta\boldsymbol{x}_0$ affects the states and the collision time on non-autonomous systems with interruptions.

On Fig. 2, $\Delta\boldsymbol{x}_0$ is an infinitesimal difference of $\boldsymbol{x}_0$, $\Delta\boldsymbol{x}_1$ and Δt_1 on Π_1 is differences of $\boldsymbol{x}_1$ and t_1 caused by $\Delta\boldsymbol{x}_0$ and $\Delta\boldsymbol{x}_2$ on $\Pi_0(t = t_2)$ is a difference of $\boldsymbol{x}_2$ caused by $\Delta\boldsymbol{x}_1$ and Δt_1. Hence from Fig. 2, we can observe the infinitesimal difference of $\boldsymbol{x}_0$ affects $\boldsymbol{x}_2$ via affecting t_1 and $\boldsymbol{x}_1$. Consequently the correct Jacobian J is actually developed as

$$J = \frac{\partial T}{\partial \boldsymbol{x}_0} = \frac{\partial T_1}{\partial t_1} \cdot \frac{\partial t_1}{\partial \boldsymbol{x}_0} + \frac{\partial T_1}{\partial \boldsymbol{x}_1} \cdot \frac{\partial T_0}{\partial \boldsymbol{x}_0}. \tag{17}$$

As is previously mentioned in Eq. (6) that T_1 depends on t_1 in non-autonomous

systems and therefore $\partial T_1/\partial t_1 \neq 0$. Moreover t_1 that is the starting time of $\boldsymbol{\varphi}_1$ depends on $\boldsymbol{x}_0$ if Π_1 is independent of the time t and then $\partial T_1/\partial t_1 \neq 0$. Above all, Eq. (17) is not the same as Eq. (15) and therefore it is required to obtain $\partial T_1/\partial t_1$ and $\partial t_1/\partial \boldsymbol{x}_0$ to get the Jacobian J. Actually from $\partial T_2/\partial t_2$ and $\partial t_2/\partial \boldsymbol{x}_0$ that is calculated by numerical differentiation,

$$\frac{\partial T_2}{\partial t_2} = \begin{pmatrix} 3.06086 \\ -0.75304 \end{pmatrix}, \quad \frac{\partial t_2}{\partial \boldsymbol{x}_0} = \begin{pmatrix} -0.18123 & 0.16996 \end{pmatrix}, \quad \frac{\partial T_1}{\partial t_1} = \mathbf{0}, \tag{18}$$

$$\begin{aligned} J &= \frac{\partial T_2}{\partial t_2} \cdot \frac{\partial t_2}{\partial \boldsymbol{x}_0} + \frac{\partial T_2}{\partial \boldsymbol{x}_2} \cdot \left(\frac{\partial T_1}{\partial \boldsymbol{t}_1} \cdot \frac{\partial t_1}{\partial \boldsymbol{x}_0} + \frac{\partial T_1}{\partial \boldsymbol{x}_1} \cdot \frac{\partial T_0}{\partial \boldsymbol{x}_0} \right) \\ &= \begin{pmatrix} 3.06086 \\ -0.75304 \end{pmatrix} \cdot \begin{pmatrix} -0.18123 & 0.16996 \end{pmatrix} \\ &\quad + \begin{pmatrix} -0.99281 & 0.36780 \\ 0.24401 & -0.09478 \end{pmatrix} \cdot \left(\mathbf{0} + \begin{pmatrix} 0 & 0 \\ 1 & 1 \end{pmatrix} \right. \\ &\qquad \left. \cdot \begin{pmatrix} 0.00000 & 0.00000 \\ -0.05423 & 0.70627 \end{pmatrix} \right) \\ &= \begin{pmatrix} -0.57469 & 0.78001 \\ 0.14162 & -0.19493 \end{pmatrix}. \end{aligned} \tag{19}$$

Here the characteristic equation according to Eq. (19) has correct multipliers.

For m-tuple systems, it is derived as follows:

$$\begin{aligned} J &= \frac{\partial T(\boldsymbol{x}_0)}{\partial \boldsymbol{x}_0} \\ &= \frac{\partial}{\partial \boldsymbol{x}_0} \left(\prod_{i=0}^{m-1} T_{m-1-i} \right) \\ &= \frac{\partial}{\partial \boldsymbol{x}_0} \left(T_{m-1}\left(t_{m-1}, \boldsymbol{x}_{m-1}\right) \circ \prod_{i=1}^{m-1} T_{m-1-i} \right) \\ &= \frac{\partial T_{m-1}}{\partial t_{m-1}} \frac{\partial t_{m-1}}{\partial \boldsymbol{x}_0} + \frac{\partial T_{m-1}}{\partial \boldsymbol{x}_{m-1}} \frac{\partial}{\partial \boldsymbol{x}_0} \left(\prod_{i=1}^{m-1} T_{m-1-i} \right). \end{aligned} \tag{20}$$

Thus for analysis of non-autonomous systems with interruptions, it is nec-

essary to consider $\partial T_{m-1}/\partial t_{m-1}$ and $\partial t_{m-1}/\partial \boldsymbol{x}_{m-1}$.

3.2. An idea to solve the problem

To obtain $\partial T_i/\partial t_i$ and $\partial t_i/\partial \boldsymbol{x}_0$, we regarded the time t_i as the state variable. Specifically let us define the system by

$$\begin{aligned} \boldsymbol{y} &= (x_0 \dots x_{n-1}, t)^\top \in \boldsymbol{R}^n \times \boldsymbol{S}^1, && (21) \\ \frac{d\boldsymbol{y}}{dt} &= \begin{pmatrix} \boldsymbol{f}_i(t, \boldsymbol{x}) \\ 1 \end{pmatrix} = \boldsymbol{g}_i(\boldsymbol{y}), \quad i = 0, \cdots, m-1. && (22) \end{aligned}$$

At this time, the system $\boldsymbol{g}(\boldsymbol{y})$ is the same as $\boldsymbol{f}(t, \boldsymbol{x})$. Putting the initial point $\boldsymbol{y}_0 = \boldsymbol{y}(0) \in \Pi'_0$ and the solution orbit $\boldsymbol{y}(t) = \boldsymbol{\Phi}(\boldsymbol{y}_0, t)$ and $\boldsymbol{y}_i(t) = \boldsymbol{\Phi}_i(t, \boldsymbol{y}_i)$, each sub map T'_i is defined as follows:

$$\begin{aligned} T'_0 \quad &: \quad \Pi'_0 \to \Pi'_1 \\ &\quad\;\; \boldsymbol{y}_0 \mapsto \boldsymbol{y}_1 = \boldsymbol{\Phi}_0 (t_1, \boldsymbol{y}_0) \\ T'_1 \quad &: \quad \Pi'_1 \to \Pi'_2 \\ &\quad\;\; \boldsymbol{y}_1 \mapsto \boldsymbol{y}_2 = \boldsymbol{\Phi}_1 (t_2, \boldsymbol{y}_1) \\ &\quad\;\; \vdots \\ T'_{m-1} \quad &: \quad \Pi'_{m-1} \to \Pi'_0 \\ &\quad\;\; \boldsymbol{y}_{m-1} \mapsto \boldsymbol{y}_m = \boldsymbol{\Phi}_{m-1} (t_m, \boldsymbol{y}_{m-1}) . \end{aligned} \qquad (23)$$

Assume that $\boldsymbol{x}(k) \in \Pi \subset \boldsymbol{R}^n$ is a location on local coordinates, then there is the projection satisfying $p(\boldsymbol{y}(k)) = \boldsymbol{x}(k)$. Let the composite map of T'_i be the

solution starting in $p^{-1}(\boldsymbol{x}(0)) = \boldsymbol{y}(0) \in \Pi_0'$. From Eq. (5),

$$p^{-1}(\boldsymbol{x}) = \boldsymbol{y} = (x_0 \dots x_{n-1}, 0)^\top \tag{24}$$

$$p(\boldsymbol{y}) = \boldsymbol{x} = (x_0 \dots x_{n-1})^\top \tag{25}$$

$$\frac{\partial p^{-1}}{\partial \boldsymbol{x}} = \begin{pmatrix} 1 & 0 & \cdots & 0 \\ 0 & 1 & \cdots & 0 \\ \vdots & & \ddots & \vdots \\ 0 & 0 & \cdots & 1 \\ 0 & 0 & \cdots & 0 \end{pmatrix}, \quad \frac{\partial p}{\partial \boldsymbol{y}} = \begin{pmatrix} 1 & 0 & \cdots & 0 & 0 \\ 0 & 1 & \cdots & 0 & 0 \\ \vdots & & \ddots & & \vdots \\ 0 & 0 & \cdots & 1 & 0 \end{pmatrix}. \tag{26}$$

From Eq. (23), the Poincaré map T is given by

$$T(\boldsymbol{x}(k), \tau, \lambda_1, \dots, \lambda_{m-1}) = p \circ T'_{m-1} \circ \cdots \circ T'_1 \circ T'_0 \circ p^{-1}. \tag{27}$$

From Eq. (23), each map T'_i only depends on the state $\boldsymbol{y}_0$ because the state $\boldsymbol{y}_0$ includes the time t. Consequently, the Jacobian matrix of the Poincaré map is given by

$$\frac{\partial T(\boldsymbol{x}_0)}{\partial \boldsymbol{x}_0} = \frac{\partial p}{\partial \boldsymbol{y}} \left(\prod_{i=0}^{m-1} \frac{\partial T'_{m-1-i}}{\partial \boldsymbol{y}_{m-1-i}} \right) \frac{\partial p^{-1}}{\partial \boldsymbol{x}_0}. \tag{28}$$

Since $\partial T'_i / \partial \boldsymbol{y}_i$ is obtained similarly to $\partial T_i / \partial \boldsymbol{x}_i$, derivative of the Poincaré map T with respect to $\boldsymbol{x}_0$ is calculated appropriately. In fact, the infinite product

part on Eq. (28) is developed as

$$
\begin{aligned}
\frac{\partial T'(\boldsymbol{y}_0)}{\partial \boldsymbol{y}_0} &= \prod_{i=0}^{m-1} \frac{\partial T'_{m-1-i}}{\partial \boldsymbol{y}_{m-1-i}} \\
&= \frac{\partial T'_{m-1}}{\partial \boldsymbol{y}_{m-1}} \cdot \frac{\partial}{\partial \boldsymbol{y}_0} \left(\prod_{i=1}^{m-1} T'_{m-1-i} \right) \\
&= \begin{pmatrix} \dfrac{\partial T_{m-1}}{\partial \boldsymbol{x}_{m-1}} & \dfrac{\partial T_{m-1}}{\partial t_{m-1}} \\ \dfrac{\partial t_m}{\partial \boldsymbol{x}_{m-1}} & \dfrac{\partial t_m}{\partial t_{m-1}} \end{pmatrix} \\
&\qquad \cdot \begin{pmatrix} \dfrac{\partial}{\partial \boldsymbol{x}_0} \left(\prod_{i=1}^{m-1} T_{m-1-i} \right) & \dfrac{\partial}{\partial t_0} \left(\prod_{i=1}^{m-1} T_{m-1-i} \right) \\ \dfrac{\partial t_{m-1}}{\partial \boldsymbol{x}_0} & \dfrac{\partial t_{m-1}}{\partial t_0} \end{pmatrix} \\
&= \begin{pmatrix} \dfrac{\partial T_{m-1}}{\partial \boldsymbol{x}_{m-1}} \dfrac{\partial}{\partial \boldsymbol{x}_0} \left(\prod_{i=1}^{m-1} T_{m-1-i} \right) + \dfrac{\partial T_{m-1}}{\partial t_{m-1}} \dfrac{\partial t_{m-1}}{\partial \boldsymbol{x}_0} \\ \dfrac{\partial t_m}{\partial \boldsymbol{x}_{m-1}} \dfrac{\partial}{\partial \boldsymbol{x}_0} \left(\prod_{i=1}^{m-1} T_{m-1-i} \right) + \dfrac{\partial t_m}{\partial t_{m-1}} \dfrac{\partial t_{m-1}}{\partial \boldsymbol{x}_0} \end{pmatrix} \\
&\qquad \begin{pmatrix} \dfrac{\partial T_{m-1}}{\partial \boldsymbol{x}_{m-1}} \dfrac{\partial}{\partial t_0} \left(\prod_{i=1}^{m-1} T_{m-1-i} \right) + \dfrac{\partial T_{m-1}}{\partial t_{m-1}} \dfrac{\partial t_{m-1}}{\partial t_0} \\ \dfrac{\partial t_m}{\partial \boldsymbol{x}_{m-1}} \dfrac{\partial}{\partial t_0} \left(\prod_{i=1}^{m-1} T_{m-1-i} \right) + \dfrac{\partial t_m}{\partial t_{m-1}} \dfrac{\partial t_{m-1}}{\partial t_0} \end{pmatrix}.
\end{aligned}
\tag{29}
$$

This result shows $\partial T/\partial \boldsymbol{x}_0$ on Eq. (28) is the same as $\partial T(\boldsymbol{x}_0)/\partial \boldsymbol{x}_0$ on Eq. (20). Therefore, the correct Jacobian is given by simple calculation process shown at Eq. (28).

4. Examples

4.1. Forced Izhikevich model

Let us consider the Izhikevich neuron model[10]. As is well known that this model is two dimensional and behaves chaotically in certain parameter setting[11] and another research[13] shows bifurcation analysis of two coupled Izhikevich neuron models. Also the model has discontinuous characteristics on

the state space. By adding an external force, the model becomes nonlinear non-autonomous system with discontinuous characteristics. Equations (30), (31) are given as follows:

$$\dot{\boldsymbol{u}}(t) = \begin{pmatrix} 0.04u_1^2 + 5u_1 + 140 - u_2 + I_0 + I\cos\omega_{\mathrm{I}}t \\ a(bu_1 - u_2) \end{pmatrix}, \tag{30}$$

$$\text{if } u_1 = \lambda_1, \text{ then } u_1 \leftarrow c,\ u_2 \leftarrow u_2 + d, \tag{31}$$

where $\boldsymbol{u} = (u_1, u_2)^\top$ is the state, and $I_0, I, \omega_{\mathrm{I}}, a, b, c, d$ and λ_1 are parameters. Equation (31) shows the jumping dynamics, and λ_1 defines the threshold values of the jumping.

We implemented the method shown in Sect. 3.2. Then we could observe the stability of fixed point and solve bifurcation problems. Figure 3 shows the bifurcation diagram in the ω_I-I plane.

Let us define each line as follows :

1. I^p: Period doubling bifurcations for p-periodic orbits.
2. G^p: Tangent bifurcations for p-periodic orbits.
3. NS^p: Neimark-Sacker bifurcations for p-periodic orbits.

In addition, the shaded area in Fig. 3 denotes period-doubling cascades[14]. The cascades continue constantly and terminated by each tangent bifurcation curve G^1. From the top side of Fig. 4, we confirm the period-adding cascade and thus we obtain the bifurcation diagram exactly. Also, we obtain the maximum Lyapunov exponent(MLE) values from the Jacobian of Poincaré map, see bottom side of Fig. 4. Above all, we could observe some fixed or chaotic attractors shown in Fig. 6.

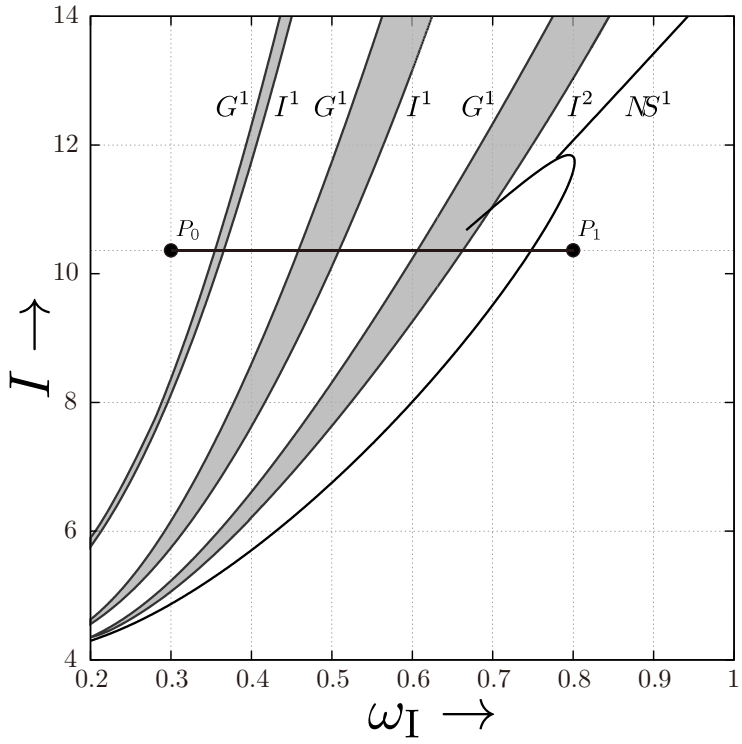

Figure 3: ω_{I} - I plane bifurcation diagram with $I_0 = 0, a = 0.2, b = 0.2, c = -50, d = 2, \lambda_1 = 30$.

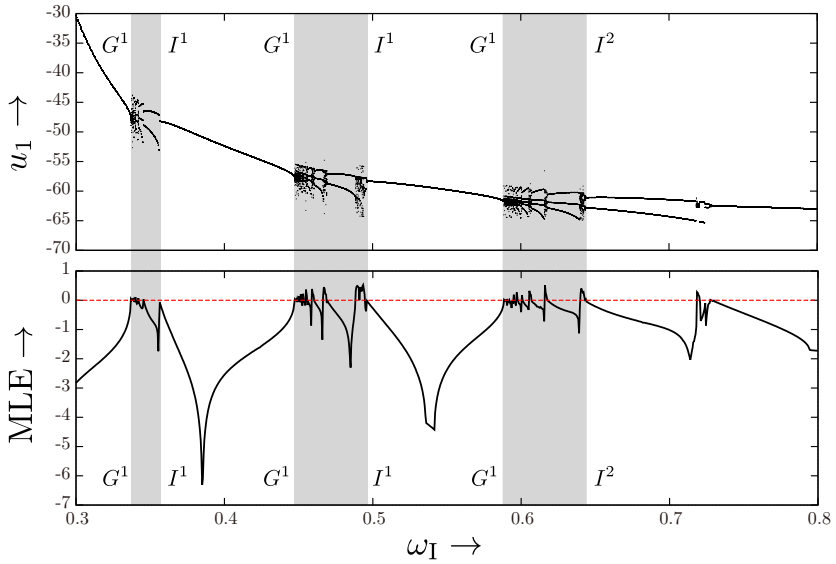

Figure 4: 1-dimensional bifurcation diagram from P_0 to P_1

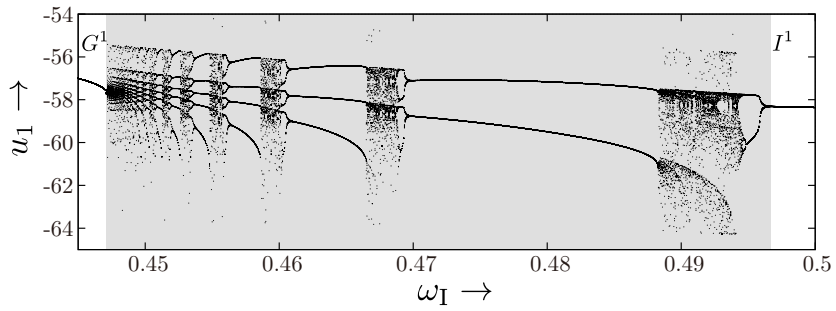

Figure 5: 1-dimensional bifurcation diagram on $0.445 \leq \omega_{\mathrm{I}} \leq 0.5$

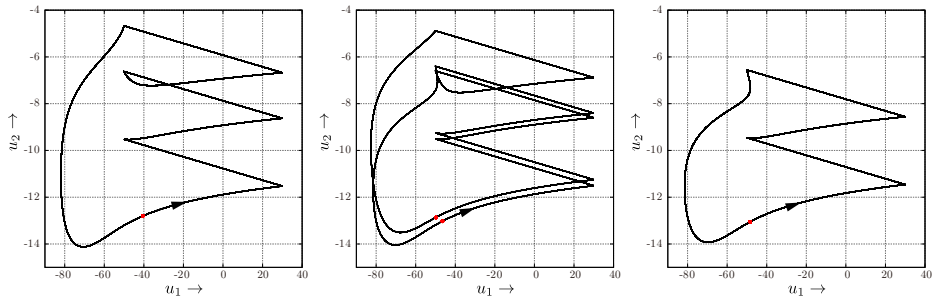

(a) $\omega_{\mathrm{I}} = 0.32$ (b) $\omega_{\mathrm{I}} = 0.35$ (c) $\omega_{\mathrm{I}} = 0.36$

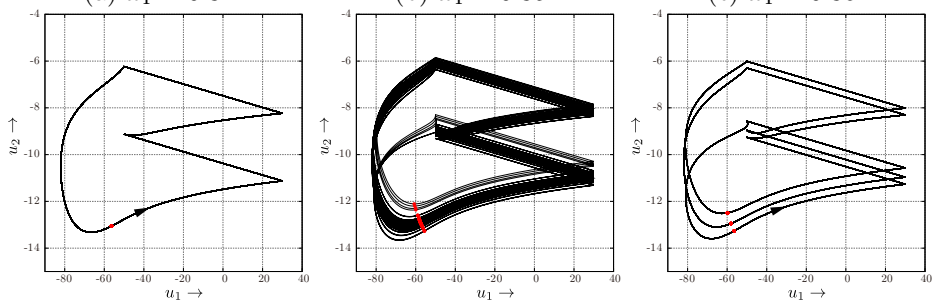

(d) $\omega_{\mathrm{I}} = 0.44$ (e) $\omega_{\mathrm{I}} = 0.45$ (f) $\omega_{\mathrm{I}} = 0.465$

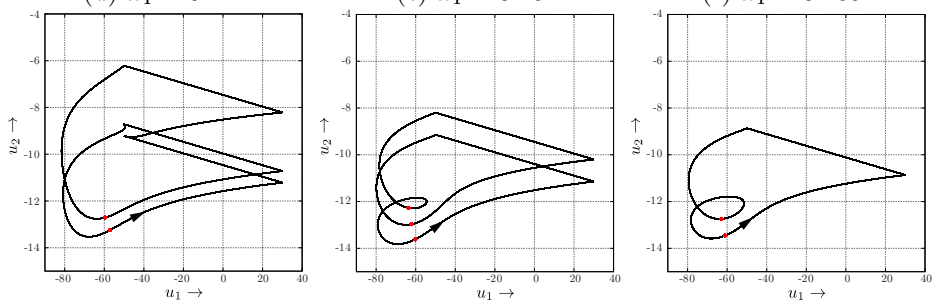

(g) $\omega_{\mathrm{I}} = 0.48$ (h) $\omega_{\mathrm{I}} = 0.63$ (i) $\omega_{\mathrm{I}} = 0.65$

Figure 6: Attractors on $I = 10$

4.2. Forced Alpazur oscillator

As the second example, we choose the Alpazur oscillator[15] and attach an alternative voltage source under a coil in series as Fig.7.

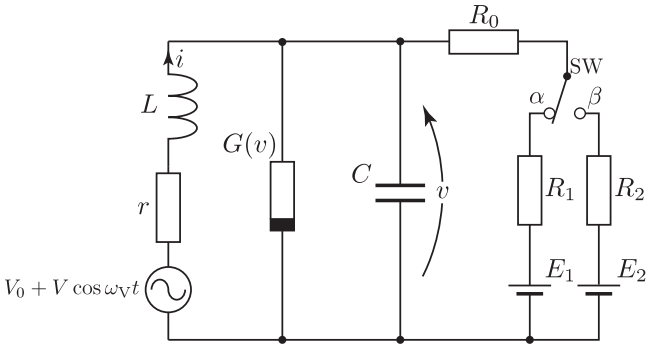

Figure 7: Forced Alpazur oscillator

The normalized circuit equation is given as follows:

$$\begin{cases} \dfrac{dv_1}{dt} &= -kv_1 - v_2 + \hat{V}_0 + \hat{V}\cos\hat{\omega}_V t \\ \dfrac{dv_2}{dt} &= \begin{cases} v_1 + (1-g_1)v_2 - \dfrac{1}{3}v_2^3 + B_1 & \text{if} \quad \text{SW is on } \alpha \\ \\ v_1 + (1-g_2)v_2 - \dfrac{1}{3}v_2^3 + B_2 & \text{if} \quad \text{SW is on } \beta \end{cases} \end{cases}, \qquad (32)$$

where, $\boldsymbol{v}_1 = (v_1, v_2)^\top$ is the state, and $k, g_1, g_2, B_1, B_2, \hat{V}_0, \hat{V}$ and $\hat{\omega}_V$ are parameters. Solution orbits of the model are switched at their boundaries

$$\begin{aligned} \partial H &= \left\{(v_1, v_2) \in \boldsymbol{R}^2 | v_2 = \lambda_2\right\} \\ \partial B &= \left\{(v_1, v_2) \in \boldsymbol{R}^2 | v_2 = \lambda_3\right\}. \end{aligned} \qquad (33)$$

Now we assume that $\lambda_3 > \lambda_2$. The behavior of the state is described as follows:

1. The flow starting from an arbitrary initial point moves within the half plane H or B, defined by Eq. (32).
2. If the flow reaches the edge ∂H or ∂B, then switching occurs.

Now we apply the method described in Sec. 3.2 to analyze bifurcation problems of this system. Figure 8 shows phase portraits of numerical solution orbits. Red points are the Poincaré mapping. Figure 8 (a)–(c) demonstrates Neimark-Sacker and period-doubling bifurcations of solutions whose trajectories touch neither ∂H nor ∂B, and then are not appeared in the original Alpazur oscillator. Since the circuit shown in Fig. 7 is physically realized by adding an AC source to the Alpazur oscillator. Figure 9 demonstrates laboratory experiments according to Fig. 8 (d)–(f).

Figure 10 is a bifurcation diagram of Eq.(32) in the $\hat{V}$-B_1 parameter plane. In this diagram, period-doubling and Neimark-Sacker bifurcations are obtained. With parameter variation of $\hat{V}$ from P_2 to P_3, the solution orbit changes its response from the quasi-periodic orbit shown in Fig. 8 (a) to 1-periodic orbit shown in Fig. 8 (b) by crossing NS^1 curve. Similarly a 2-periodic orbit at P_4 shown in Fig. 8 (c) is given be crossing I^1. Now we should note that a period-doubling bifurcation corresponding to I^1 between P_5 to P_6 is computed concretely. In addition to this fact, corresponding numerical and experimental results of Fig. 8 (d),(e), and 9 (a),(b), we validate that our numerical method for switched periodic orbits works well. Also we observe chaotic attractors both numerically and experimentally as shown in Fig. 8 (f) and 9 (c).

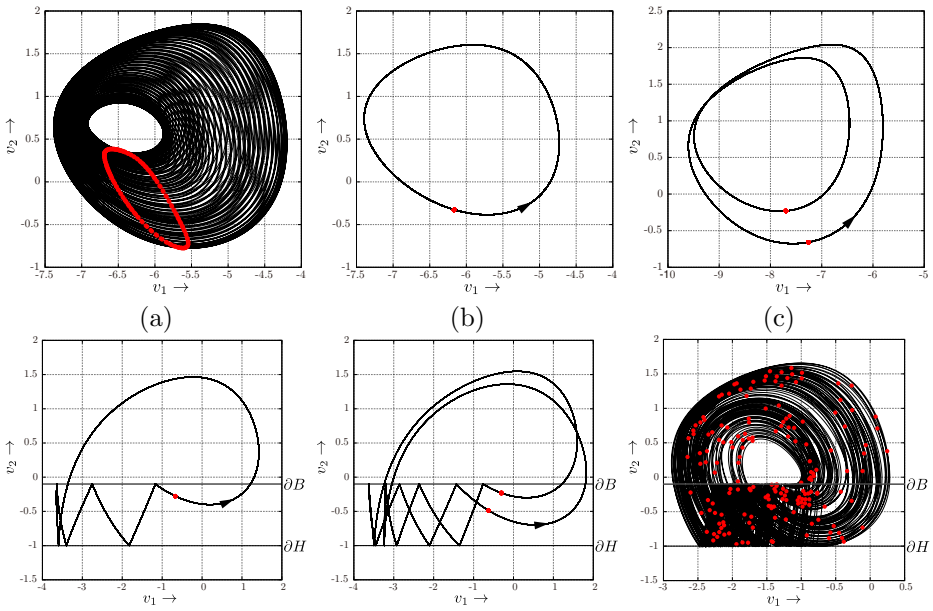

Figure 8: Phase portraits by numerical computation with $k = 0.1, g_1 = 0.2, g_2 = 2.0, B_2 = 5, \lambda_2 = -1.0, \lambda_3 = -0.1, \hat{V}_0 = 0, \hat{\omega}_{\rm V} = 1.26$, (a) $P_2 : \hat{V} = 0.5, B_1 = 6$, (b) $P_3 : \hat{V} = 0.65, B_1 = 6$, (c) $P_4 : \hat{V} = 1, B_1 = 8$, (d) $P_5 : \hat{V} = 2.5, B_1 = 0.1$, (e) $P_6 : \hat{V} = 2.5, B_1 = -0.1$ and (f) $P_7 : \hat{V} = 0.5, B_1 = 6$.

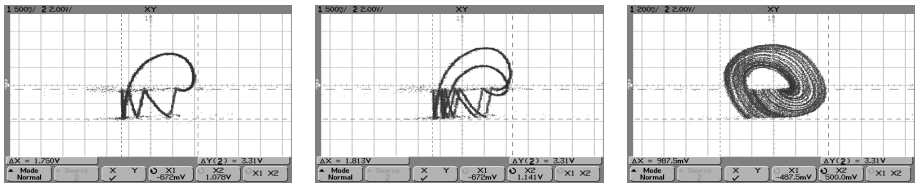

Figure 9: Laboratory experiments with $L = 50[\text{mH}], r = 113[\Omega], C = 0.09[\mu\text{F}], R_0 = 0[\Omega], R_1 = 811.7[\Omega], R_2 = 212.9[\Omega], E_2 = 6[\text{V}], V_0 = 0[\Omega], \omega_{\rm V} = 1.88 \times 10^3[\text{rad/s}]$. (a) $V = 9[\text{V}], E_1 = -3.0[\text{V}]$. (b) $V = 9[\text{V}], E_1 = -4.0[\text{V}]$. ($i$: 24.0mA/div, v : 2.0V/div) (c) $V = 0.4[\text{V}], E_1 = 0.1[\text{V}]$. ($i$: 9.6mA/div, v : 2.0V/div)

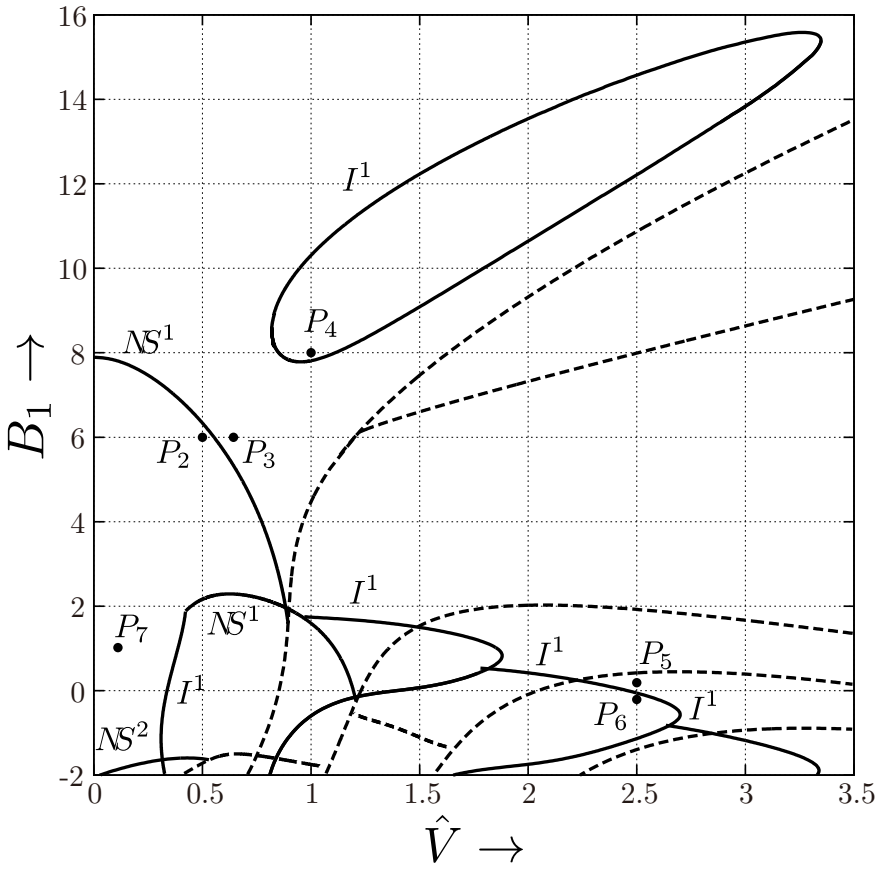

Figure 10: $\hat{V}$ - B_1 plane bifurcation diagram with $k = 0.1, g_1 = 0.2, g_2 = 2.0, B_2 = 5, \lambda_2 = -1.0, \lambda_3 = -0.1, \hat{V}_0 = 0, \hat{\omega}_{\rm V} = 0.2$

5. Conclusion

We have proposed an analysis method for a bifurcation problem on the non-linear non-autonomous system with discontinuous characteristics. The method spuriously transforms the non-autonomous system to an autonomous system by including the time t to the state. By transforming, we could consider the effect of the starting time t_m at the local section Π_m on a non-autonomous system and thus we could obtain the stability of the solution exactly. For an application of the method, we analyzed the forced Izhikevich model which has a discontinuous characteristic on the state space. We could obtain the bifurcation set exactly and found that the model has three types of bifurcations; period-doubling, tangent and Neimark-Sacker. In addition, the system shows some period adding cascades and chaotic attractor. For another application, we proposed the model for forced Alpazur oscillator which has discontinuous characteristics on the space of time derivative of the state Also we could obtain the bifurcation diagram exactly and found there are two types of local bifurcations; period-doubling and Neimark-Sacker bifurcation, and global bifurcation; grazing bifurcation. Moreover we confirmed the results with labo experiments.

From two examples, we found the method can be applied to any pattern which has discontinuous characteristics.

Acknowledgements

This research is partially supported by JSPS KAKENHI 25420373.

References

[1] H. Kawakami, K. Kobayashi, A computation of periodic solutions of non-linear autonomous systems, in: Proc. ISCAS, vol. 79, 44–45, 1979.

[2] H. Kawakami, Bifurcation of periodic responses in forced dynamic nonlinear circuits: Computation of bifurcation values of the system parameters,

Circuits and Systems, IEEE Trans. on 31 (3) (1984) 248–260, ISSN 0098-4094.

[3] T. Ueta, G. Chen, T. Yoshinaga, H. Kawakami, A numerical algorithm for computing Neimark-Sacker bifurcation parameters, in: Proc. ISCAS 1999, vol. 5, IEEE, 503–506, 1999.

[4] S. Doole, S. Hogan, A piece wise linear suspension bridge model: nonlinear dynamics and orbit continuation, Dynamics and Stability of Systems 11 (1) (1996) 19–47.

[5] S. Banerjee, P. Ranjan, C. Grebogi, Bifurcations in two-dimensional piecewise smooth maps-theory and applications in switching circuits, Circuits and Systs I: Fundamental Theory and Applications, IEEE Trans. on 47 (5) (2000) 633–643.

[6] M. Bernardo, M. Feigin, S. Hogan, M. Homer, Local analysis of C-bifurcations in n-dimensional piecewise-smooth dynamical systems, Chaos Solut. and Fract. 10 (11) (1999) 1881–1908.

[7] T. Kousaka, T. Ueta, H. Kawakami, Bifurcation of switched nonlinear dynamical systems, IEEE Trans. Circuits Systs. 46 (7) (1999) 878–885.

[8] T. Ueta, H. Kawakami, I. Morita, A Study of the Pendulum Equation with a Periodic Impulsive Force: Bifurcation and Control, IEICE trans. on fundamentals of electronics, communications and computer sciences 78 (10) (1995) 1269–1275.

[9] M. Di Bernardo, C. Budd, A. Champneys, Grazing and border-collision in piecewise-smooth systems: A unified analytical framework, Physical Review Letters 86 (12) (2001) 2553.

[10] E. M. Izhikevich, et al., Simple model of spiking neurons, IEEE Trans. neural networks 14 (6) (2003) 1569–1572.

[11] A. Tamura, T. Ueta, S. Tsuji, Bifurcation Analysis of Izhikevich Neuron Model, Dynamics of Continuous, Discrete and Impulsive Systems 16 (6) (2009) 849–862.

[12] D. Ito, T. Ueta, T. Kousaka, J. Imura, K. Aihara, Controlling Chaos of Hybrid Systems by Variable Threshold Values, Int. J. of Bifurcation and Chaos 24 (10) (2014) 1450125.

[13] D. Ito, T. Ueta, K. Aihara, Bifurcation analysis of two coupled Izhikevich Oscillators, in: Proc. NOLTA2010, Krakow, 627–630, 2010.

[14] P. T. Piiroinen, L. N. Virgin, A. R. Champneys, Chaos and period-adding; experimental and numerical verification of the grazing bifurcation, J. Nonlinear Science 14 (4) (2004) 383–404.

[15] H. Kawakami, R. Lozi, Switched Dynamical Systems–dynamical of a class of circuits with switch–, in: Proc. RIMS Conf."Structure and Bifurcations of Dynamical Systems," (ed.) S. Ushiki, World Scientific, 39–58, 1992.